1982A&A...113..285N

Astron. Astrophys. 113, 285–302 (1982)

ASTRONOMY AND ASTROPHYSICS

Structure and Dynamics of Supersonic Jets

M. L. Norman, L. Smarr*, K.-H. A. Winkler, and M. D. Smith**

MUNAC (Munich Numerical Astrophysics Coalition), Max-Planck-Institut für Physik und Astrophysik, Institut für Astrophysik, Karl-Schwarzschild-Strasse 1, D-8046 Garching bei München, Federal Republic of Germany

Received March 8, accepted May 14, 1982

Summary. The Blandford and Rees (BR) beam model for extragalactic radio sources is critically examined within the context of axisymmetric, nonrelativistic ideal gas dynamics. Thus we assume that radio jets contain thermal matter that governs the structure and dynamics of the jet. We conduct numerical experiments that study the structure and stability of the 3 basic jet components conceived by BR-beam, working surface, and cocoon – for various beam Mach numbers and temperature ratios with respect to a constant ambient medium (the intergalactic medium). Jets are established by continuously injecting a collimated supersonic beam of gas into, and in pressure equilibrium with, the ambient medium.

We find that such beams propagate efficiently at high Mach numbers ($M_b \gtrsim 6$). At the working surface, the beam is decelerated by a Mach-disk shock front which is in general much stronger than the bow shock running ahead of the jet. Backflow from the working surface builds an extensive cocoon surrounding the beam provided the beam/medium temperature ratio is high ($T_b/T_m \gtrsim 10$). For sufficiently "hot", high Mach number jets the cocoon backflow is supersonic, raising the possibility of a wholly stable supersonic jet. At lower Mach numbers and temperature ratios, the backflow is less strong, producing lobes instead of cocoons. Lobes and low velocity cocoons are generally Kelvin-Helmholtz (KH) unstable and mix with the ambient gas at a ragged boundary. The dominant KH wavelength is 1–2 jet diameters; the perturbations originating through a Rayleigh-Taylor instability at the working surface driven by a feedback mechanism that links beam, working surface and cocoon.

Waves and instabilities on the jet boundary generally perturb the beam, which is itself stable except for Mach numbers approaching unity. We find that perturbations set up oblique internal shock waves in the beam with a rather regular spacing of 1–2 jet diameters quite independent of the beam Mach number. A Kelvin-Helmholtz unstable beam is also found to develop spatially quasi-periodic shocks with a spacing of ~ 2 beam diameters. The shocks separate regions of supersonic and subsonic flow in a beam with a repeating cavity/nozzle structure. Nozzle breakup is identified as a mechanism that efficiently entrains ambient gas into the beam. We suggest that quasi-periodic shockwaves that arise in regions of global jet instability are a possible explanation for the knots observed in the M87 jet.

Send offprint requests to: M. L. Norman

* Permanent address: Depts. of Astronomy and Physics, Urbana, Illinois, USA

** Permanent address: Dept. of Physics, Univ. of Illinois, Urbana, Illinois and Dept. of Astronomy, Univ. of Maryland, College Park, Maryland, USA

Key words: galaxies: double radio sources – radio jets – gas dynamics: supersonic flow – shockwaves – Rayleigh-Taylor/Kelvin-Helmholtz-instabilities

I. Problem Statement

How does a supersonic beam of gas bore its way through quiet gas? What are the structural and stability properties of the beam end? Is the beam stable against the disrupting effects of nonlinear Kelvin-Helmholtz instabilities? Do cocoons exist, and what is their role in beam propagation? How is beam collimation preserved? Is quiet gas entrained in the jet? Can quasi-periodic structures such as knots be understood from a fluid dynamical model? Answering these questions is central to deciding whether the widely accepted "beam model" proposed by Blandford and Rees (1974, 1978), and Scheuer (1974) is a viable explanation for the radio jets observed in many galaxies (Miley, 1980), and for determining whether the jet is a workable "energy pipe" for powering extended radio lobes and hot spots.

We report here the results of recent numerical experiments that address and answer these questions within the framework of axisymmetric, ideal compressible flow. In Sect. II we review the physical assumptions and problem parameters; we set up the problem; and we briefly describe the calculation technique. In Sect. III we compare the code against laboratory observations of the steady flow pattern arising in a supersonic underexpanded jet. In Sect. IV we begin our study of supersonic pressure-matched jets, more appropriate to the astrophysical situation. The jet's three basic structural components are introduced: working surface, cocoon, and beam. The structure and stability of each component are then examined in greater detail in Sects. V–VII respectively. Fully self-consistent structures and instabilities arising in the jet and working surface are described, and displayed by computer graphical output. Finally, in Sect. VIII we answer the questions raised at the beginning of this paper within the limitations of our model calculation. Astrophysical implications are discussed. In an Appendix we make some comments on numerical effects and uncertainties inherent in the calculations, primarily regarding the flow boundaries and the modelling of unstable shear surfaces and layers.

This is the first in a series of papers on this problem. Herein we examine the results of the numerical calculations. In the second paper we make detailed comparison to observations of jets, knots, and hot spots. In a third paper we use analytic and perturbation arguments to verify the features we have discovered numerically and to explain them in terms of simple physical arguments.

© European Southern Observatory • Provided by the NASA Astrophysics Data System

1982A&A...113..285N

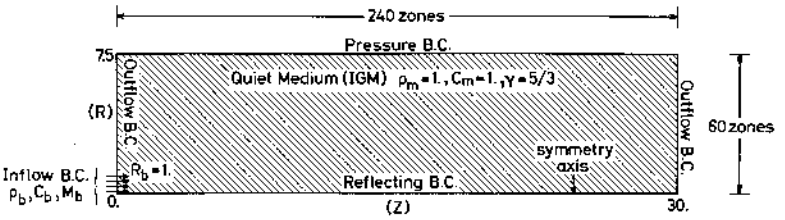


Fig. 1. Specifications for the computational domain, indicating the types of flow boundary conditions used. The pressure boundary is maintained at the initial IGM pressure. A collimated supersonic beam of gas of density ϱ_b, sound speed C_b, and Mach number M_b is continuously admitted through an aperture of radius R_b into quiet gas of density $\varrho_m=1$ and sound speed $C_m=1$. $\gamma=5/3$ for both gases

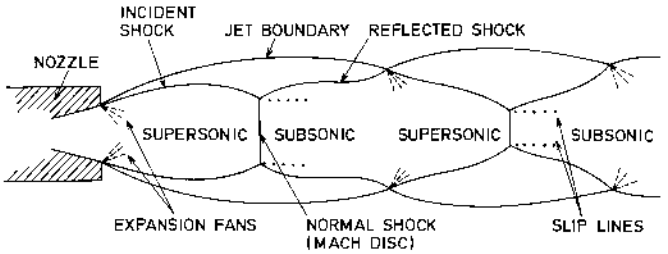


Fig. 2. Sketch of jet structure behind a highly underexpanded nozzle, adapted from Adamson and Nicholls (1959)

II. Setup of Numerical Experiments

In this paper we are not concerned with the origin of collimated jets, but rather assume them, and study their propagation, structural, and stability properties as they bore through the constant density and pressure intergalactic medium (IGM). We assume non-relativistic gas dynamics is a valid approximation for both jet gas and IGM; i.e. following Blandford and Rees (1974) we invoke the presence of small but dynamically unimportant magnetic fields so that the ion Larmor radius is much smaller than the macroscopic scales of interest. We are thus tacitly assuming that radio jets contain thermal matter that governs the dynamics of the jet. It is this thermal component that we model. While neglecting the effects of bulk relativistic motions and magnetic fields may be unrealistic for some radio jets, our current knowledge of their internal constitution is so scanty that we feel a rather more complete investigation of the consequences of the conservation laws embodied in the Euler equations is justified. Finally, we consider axisymmetric flow, hence nonaxisymmetric modes such as the fluting and the "garden hose" instabilities of the jet cannot be addressed.

Define a cylindrical coordinate system R, Z; where Z is an axis of symmetry aligned with the jet axis and R is the cylindrical radius. We integrate the Newtonian equations of ideal compressible gas dynamics by time-explicit finite differencing techniques. Shock waves are treated by the methods of monotonicity and artificial viscosity. Two important aspects of the numerical scheme deserve mentioning. Wilson conservative Eulerian hydrodynamics is employed (Wilson, 1978), improved by second-order monotonic advection (Winkler et al., 1982). Of crucial importance to this application is the use of LeBlanc interface – tracking (Norman, 1980), which numerically treats the contact discontinuity between the jet and IGM gases as a true dynamic fluid boundary. Without the employment of LeBlanc interfaces, surface waves and instabilities could not be studied accurately with our present code. This code has been extensively tested against well-known solutions. These results will be reported elsewhere.

We consider the following initial-boundary value problem: continuously admit collimated beam gas of density ϱ_b, sound speed C_b, and Mach number M_b through an aperture of radius R_b into a cylindrical chunk of quiet medium gas of density ϱ_m, and sound speed C_m (see Fig. 1). Both gases have specific heat ratio $\gamma=5/3$. In practice the problem domain encompasses $0<R<7.5\ R_b$, $0<Z<30\ R_b$. The flow boundary conditions used for the computations are indicated in Fig. 1. The computational grid has $60\times240=14{,}400$ uniform zones. A typical evolution of 10,000–12,000 time-steps requires 2–3 h of CRAY-1 cpu time.

We choose $\varrho_m=C_m=R_b=1$, thus the reference luminosity $L_m\equiv\varrho_m R_b^2 C_m^3=1$. With this choice of scaling, the beam parameters ϱ_b, C_b, and M_b; and the beam kinetic luminosity $L_b=\pi R_b^2\varrho_b M_b^3 C_b^3$, are dimensionless. We set the pressure ratio of the incoming beam gas to the IGM to some constant K (usually 1). This imposes the further constraint that $\varrho_b C_b^2=K\varrho_m C_m^2$. For a given K the parameter space then reduces to the beam/medium density ratio ϱ_b, and the beam Mach number M_b. Because the only length scale in the problem is the beam radius R_b, we can scale our results from laboratory jets to cosmic jets. The unit of time is $R_b/C_m=1$, the time it takes sound to move R_b in the external medium.

III. Underexpanded Laboratory Jets

The study of jets in the laboratory is nearly a century old (Mach and Salcher, 1889; Hartmann and Lazarus, 1941; Ladenburg et al., 1949; Love et al., 1959; Adamson and Nicholls, 1959; Moe and Troesch, 1960; Abbett, 1971; Fox, 1974; Chang and Chow, 1974). We review the relevant knowledge gleaned from laboratory experiments on jets and then perform a numerical calculation of such a jet to compare with the experimental data.

Jet flows can be either subsonic or supersonic. The qualitative structure of such jets are entirely different. In a subsonic jet (see, e.g. Tennekes and Lumley, 1972) the flow, although initially parallel and in pressure equilibrium with its surroundings, increases in cross sectional area as it propagates. This is because the slip discontinuity between the jet material and the quiet medium is highly unstable to Kelvin-Helmholtz modes. Because the flow on both sides of the slip is subsonic, the eddies can complete several turnovers as they are advected downstream, thus effectively entraining large amounts of the quiet medium into the jet. A simple argument (Tennekes and Lumley, 1972) shows that the opening angle of the jet is 3.8 deg.

A supersonic jet, in contrast, has a wealth of internal structure caused by the existence of shock waves (Courant and Friedrichs, 1948). The global structure of a supersonic air jet depends strongly on the ratio K of the jet pressure to the ambient pressure. (Air jets are assumed to have the same density as the atmosphere, so the pressure ratio is the variable). If this ratio K is greater than, equal to, or less than unity, the jet is referred to as underexpanded, matched, or overexpanded, respectively.

The underexpanded jet seems to be easier to study experimentally and comes up more often in application, since one usually has

© European Southern Observatory • Provided by the NASA Astrophysics Data System

1982A&A...113..285N

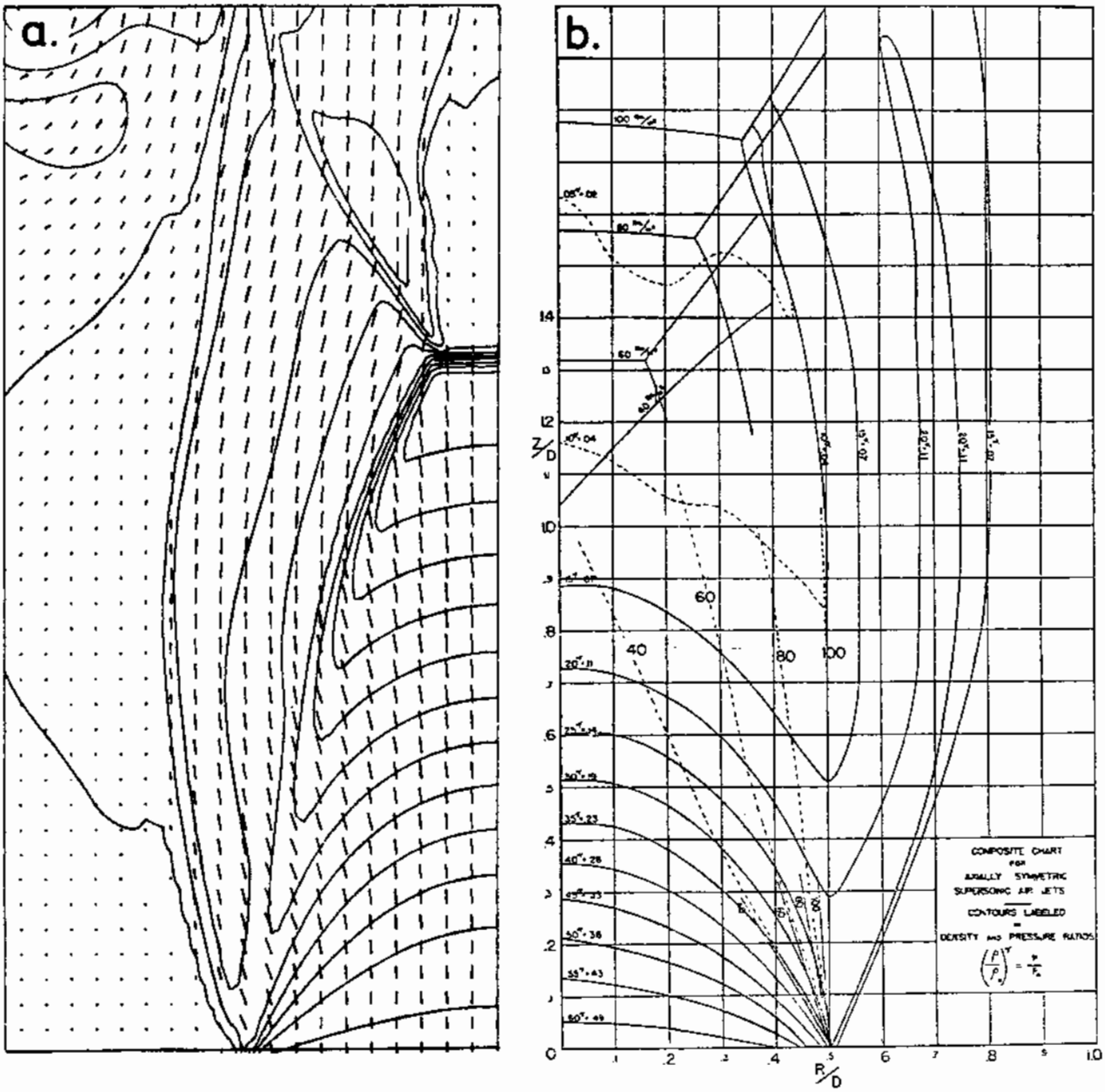
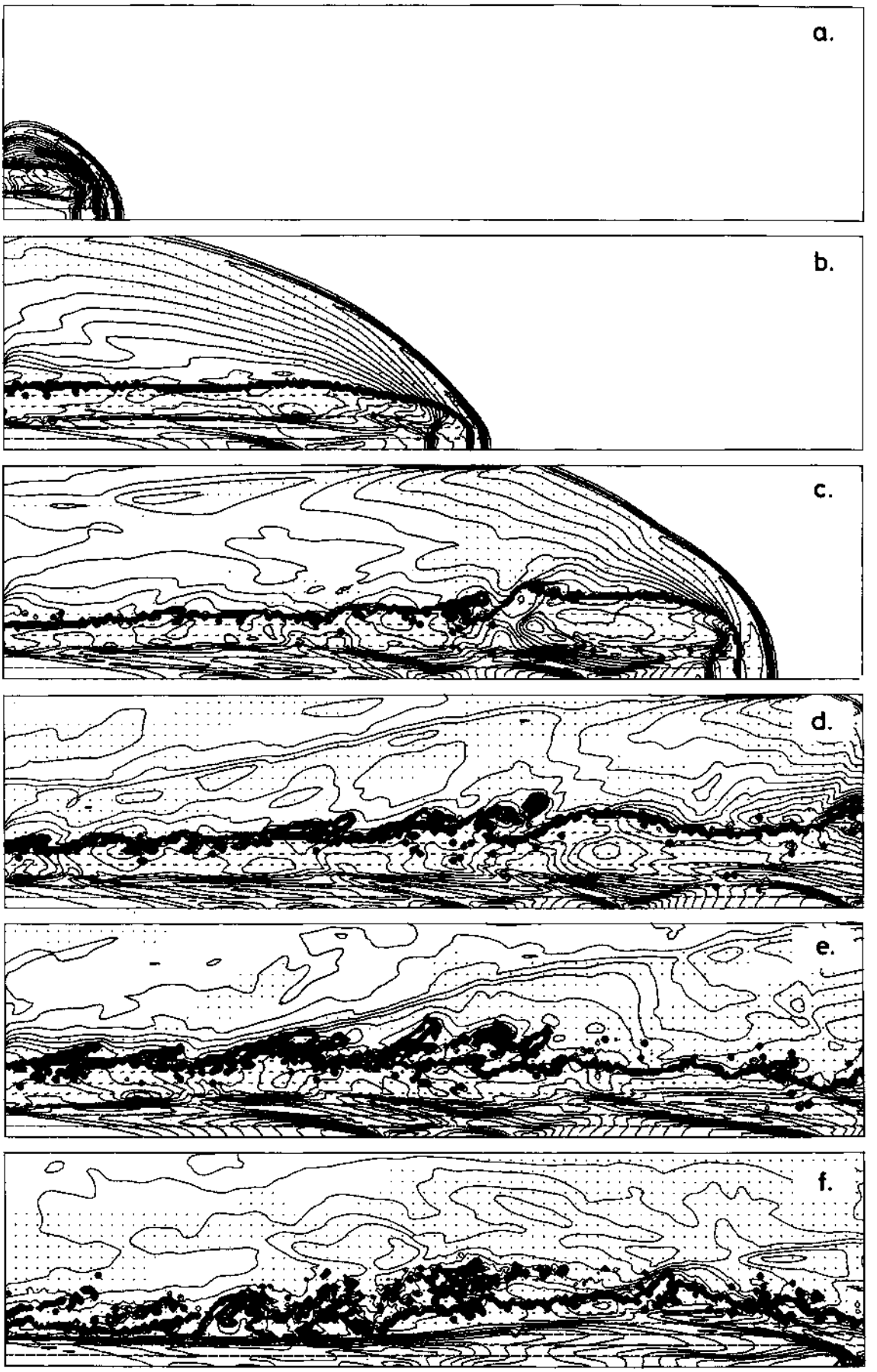


Fig. 3. a Density contours and velocity vectors of the numerical solution of a $K=2.75$ underexpanded jet, to be compared with the $P_0=60$ lbs/in^2 curves in **b**. This run used a grid of 60×180 zones. **b** Composite chart of experimental results on the flow pattern in underexpanded axially symmetric, supersonic air jets, from the review paper by Ladenburg et al. (1949). Contour lines are labelled in density and pressure ratios ($(\varrho/\varrho_0)^\gamma=P/P_0$), where ϱ_0 and P_0 are the reservoir density and pressure, respectively. Superposed are the triple-shock configurations for four choices of reservoir pressure: $P_0=40$, 60, 80, and 100 lbs/in^2 corresponding to pressure ratios of 2.0, 2.75, 3.49, and 4.23 at the nozzle (Mach 1)

a high pressure reservoir as the source for the jet and a lower pressure receiver into which the jet expands. Figure 2 shows schematically the features found in a high pressure ratio ($K>1$) underexpanded jet (adapted from Adamson and Nicholls, 1959), while Fig. 3b (reproduced from the review paper of Ladenburg et al., 1949) shows contours of density and pressure in the jet as measured experimentally. As the high pressure air comes out of the orifice (diameter D), it undergoes a Prandtl-Meyer expansion to decrease its pressure and match on to the atmospheric pressure. This causes the jet boundary to expand and a rarefaction to begin down the centerline of the jet. However, the characteristic lines reflecting off the jet boundary soon intersect, creating the incident imbedded shock which causes a reconverging of the jet. This incident shock is revealed by the doubling back of the density-pressure contours in the rarefying jet as seen in Fig. 3b. The incident shock attempts to reflect off the symmetry axis. If the pressure ratio is small, then the shock is weak and approaches the axis so obliquely that it can make a regular reflection off the axis, as seen in Fig. 3b for the jet pressure equal to 40 lb/in^2, $K=2.0$. For higher pressure ratios, the strong shock makes a small angle with

© European Southern Observatory • Provided by the NASA Astrophysics Data System

1982A&A...113..285N



© European Southern Observatory • Provided by the NASA Astrophysics Data System

1982A&A...113..285N

Table 1. Survey parameters and summary

M_b	ϱ_b	C_b	L_b	Comments
6	0.1	10	2145	Extensive cocoon, supersonic backflow, vortex shedding, stable beam, internal shocks
3	0.1	10	268	Unstable cocoon/lobe, vortex shedding, stable beam, internal shocks
1.5	0.1	10	33	No cocoon, unstable lobe, stable beam
6	1.0	1.0	679	Cocoon "roll-up", vortex shedding, stable beam, internal shocks
1.5	1.0	1.0	11	No cocoon, unstable lobe, unstable beam, entrainment

respect to the axis normal, and must reflect at a triple point off a Mach disk; see Fig. 3b for jet pressure >60 ($K>2.75$). The Mach disk is a circular (because of the assumed axisymmetry) shock front which is stationary in the flow. The incident shock meets this shock and produces a reflected shock. To satisfy the jump conditions, a slip line (a surface along which tangential velocity is discontinuous, but normal component of velocity and pressure are continuous) must join this triple point (see Fig. 2).

In the laboratory, this entire flow structure is attached to the orifice. The jet itself continues downstream beyond the Mach disk, going through a series of repeated expansions and contractions (Fig. 2) causing repeated supersonic – subsonic transitions, until finally the jet remains subsonic and mixes with the atmosphere.

In order to test the accuracy of the numerical model, we computed a $K=2.75$ underexpanded jet. The results are shown in Fig. 3a, and can be compared directly to the 60 lb/in^2 curves in Fig. 3b. The key measurable quantities are the distance downstream from the nozzle of the Mach disk, and its radius to the shock triple point. The experimental numbers fall within the limits set by our smeared-out shock width. We conclude that our code can reproduce all the qualitative features of this jet flow in good quantitative detail.

We have spent considerable time on discussing the underexpanded supersonic jet for two reasons. First, it shows our code can resolve all the features of these known flows. Second, it will turn out to be the solution for how a supersonic jet ends itself in cosmic radio lobes.

IV. Pressure-matched Jets

In contrast to underexpanded laboratory jets, the jets seen in radio galaxies appear in many cases (Miley, 1980) to be in pressure equilibrium with the surrounding gas (intergalactic medium IGM). These pressure confined jets can be modelled by choosing $K=1$. Such matched jets may have a density contrast (ϱ_b) and therefore sound speed (temperature) contrast (C_b) with the IGM. We model these jets by assuming the incoming flow is parallel with Mach number M_b. Actual radio galaxy jets have small opening angles of 1°–3°, perhaps indicating a slight pressure mismatch. We ignore this slight deviation from parallelism, returning to it in a later paper in this series.

Steady flow in a pressure-matched beam of slowly varying cross-section was first studied in the one-dimensional approximation by Blandford and Rees (1974). However, when they considered the region where the jet ended (the working surface) they thought in two dimensions, for the one-dimensional analysis cannot apply[1]. They deduced that the jet would end at a contact discontinuity separating the jet material from the IGM. This discontinuity would propagate supersonically with respect to the IGM sound speed (C_m) and therefore a bow shock would form in front of the contact surface. Because the velocity of the contact is slower than the velocity of the beam material, a shock internal to the beam must form to decelerate the beam material before it hits the contact. Concerning the subsequent motion of the shocked beam material, they suggested that the flow would move backward along the beam, forming a cocoon. Thus, Blandford and Rees proposed three basic structural components of a supersonic, pressure-matched jet: beam, working-surface, and cocoon. This simple picture (see their Fig. 2) is verified by our detailed calculations.

Rayburn (1977) has previously used a very coarse-grid numerical code ($10\times 20=200$ grid points) to give a first guess as to the two dimensional structure of the flow, but was unable to find much internal structure beyond that already implied in Blandford and Rees' analysis. Furthermore, his code was not capable of studying the stability of interfaces in the flow which are crucial to the dynamical behaviour of the jet, or of allowing the jet to propagate off the end of the grid so as to study the long-term global stability of the beam.

By going to very high resolution ($\sim 15{,}000$ grid points), we have been able to resolve many important features of the flow. We have made 5 detailed runs listed in Table 1. They span a large range in luminosity for both hot and cold jets. Before treating these in detail, we first show a time history of a high Mach number ($M_b=6$), hot ($\varrho_b=0.1$), high luminosity ($L_b=2155$) jet boring its way through the grid and off the other side. Figures 4a–4c show the establishment and the propagation of the jet before the working surface exits the problem domain. The major features predicted by Blandford and Rees are seen: beam, contact discontinuity, cocoon, and bow shock. Figure 4d–f show the behaviour of the jet after the working surface leaves the problem domain. Loss of the working

1 In one dimension, there are only plane shock waves and contact discontinuities. A one-dimensional supersonic "beam" would meet the IGM at a (plane) contact discontinuity, with a (plane) internal shock and a (plane) external shock receding from it in opposite directions with precisely the shock strengths needed to bring the unshocked internal and external flows to rest with respect to the contact discontinuity. Only in two or three dimensions can the shocks and contact discontinuity remain at rest with respect to each other because the postshock gas can escape sideways. As a result, these flow discontinuities are no longer planar

Fig. 4a–f. Time history of a hot ($\varrho_b=0.1$), Mach 6 jet boring through the IGM. Density contours are spaced by a factor of 1.2. Velocity vectors are drawn at every 3rd grid-point. A 60×240 grid is used. **a–c** Establishment and propagation of the jet before the working surface leaves the problem domain. As detailed in Fig. 5, beam, internal shock, bow shock, contact discontinuity, and cocoon are all visible. **d–f** Disruption of the cocoon via nonlinear Kelvin-Helmholtz instabilities induced by the working surface leaving the problem domain (see Sect. VI.c)

© European Southern Observatory • Provided by the NASA Astrophysics Data System

1982A&A...113..285N



Fig. 5. Density contours showing details of a hot ($\varrho_b=0.1$), Mach 6 jet. Velocity vectors are drawn at every grid point. Beam gas is admitted at the lower left-hand corner with velocity 19, which streams to the right where it is shock decelerated and heated at the Mach disk. The working surface moves forward with velocity 4.2, setting up a bow shock in the IGM. High pressure beam cap gas flows first laterally and then back along the beam to feed the cocoon, here flowing to the left with velocity −7.1 (Mach 1.6). Vorticity generated at the triple-shock wave configuration appears as vortical flow in the cocoon. Structural changes near the beam cap perturb the contact discontinuity; perturbations grow via the Kelvin-Helmholtz instability as they advect back along the jet. Perturbations transmitted to the beam by the cocoon set up oblique internal shock waves. High density knots occur behind each shock reflection

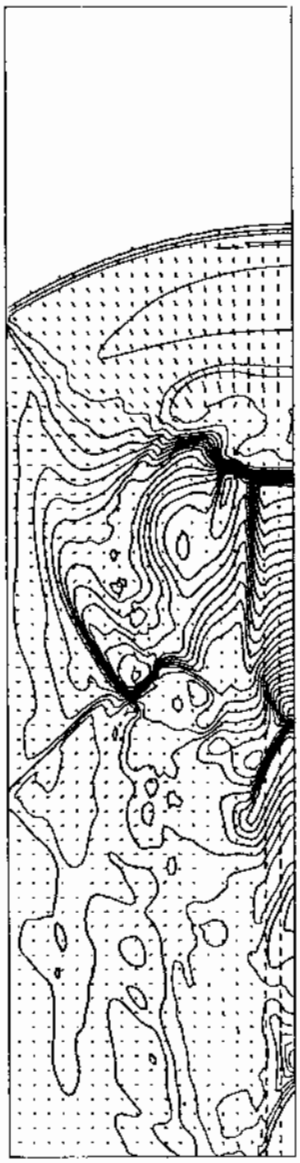


Fig. 6. Pressure contours of a hot ($\varrho_b=0.1$), Mach 3 jet, showing the greater shock strength of the Mach disk compared with the bow shock. Also shown are momentum vectors at every 3rd gridpoint

surface induces the growth of Kelvin-Helmholtz instabilities on the cocoon/IGM interface and the onset of mixing of the two gases. The structure and mechanics of the working surface are discussed in the next section. The working surface supplies gas to the cocoon, whose structure and stability are examined in Sect. VI. The beam is considered last in Sect. VII because its structure and stability are influenced by the properties of the cocoon.

V. Working Surface

We now describe in detail the propagating head of the jet. For the moment we focus our discussion on the hot ($\varrho_b=0.1$) Mach 6 jet shown in Fig. 5. Later, the effects of varying the beam parameters are considered.

© European Southern Observatory • Provided by the NASA Astrophysics Data System

1982A&A...113..285N

a) Structure

As predicted by Blandford and Rees (1974), a contact discontinuity separates the leading bow shock in the IGM from a shock configuration interior to the jet which decelerates the beam to the velocity of the contact discontinuity. The shocked beam gas is indeed diverted into a cocoon. However, our two-dimensional numerical experiment reveals an important qualitatively new feature of this hydrodynamic flow: the beam terminates itself as an underexpanded jet with a Mach disk configuration as described for supersonic laboratory jets in Sect. III. A typical situation is displayed in Fig. 5. Restricting our attention for the moment to the right-most part of the jet, we see closed density contours indicating low-pressure centers in the cocoon. The beam responds to the low pressure by expanding away from the axis, creating the "rarefaction valley". Once pressures have equalized, the expansion is halted by the so-called incident shock, which converges toward the axis until it meets at a triple point a Mach disk shock, reflected shock, and slipline discontinuity. The beam material below the slip line is shocked by the Mach disk and remains in the beam cap as a stagnant region of hot high pressure gas. The rest of the beam gas is shocked by first passing through the incident shock and then through the reflected shock. It emerges above the slipline and is diverted upward by the high pressure beam cap gas. This gas then flows around a low pressure center and feeds the cocoon directly.

The key point is that a low pressure center must form to provide a pressure gradient which can change the direction of the beam velocity by 180°. This low pressure torus (considering the axisymmetry of the problem), sits above the Mach disk and serves as the ambient low pressure which causes the beam to become underexpanded in the first place. This nonlinear self-consistent configuration of low pressure "eye" and triple shock structure is the way in which the equations of gas dynamics allow a supersonic beam to terminate itself. The elucidation of this structure indicates the power of doing full scale numerical experiments on gas dynamical flows.

The major differences compared with the laboratory underexpanded jet are twofold. First, our Mach disk configuration propagates by self-consistently generating an "effective orifice" several jet radii backward from the head of the jet. Second, as a consequence of this propagation, in the rest frame of the Mach disk the IGM is flowing supersonically towards it. This sets up the leading bow shock and swept back contact discontinuity which "seals off" the beam and prevents the repeated Mach disks seen in Fig. 2.

We next consider the relative strengths of the shocks: the bow shock, the Mach disk shock, the incident shock, and the reflected shock. A simple one-dimensional argument would say that the ram pressures of the beam and the IGM must balance across the beam area in the rest frame of the bow shock. Let $V=M_bC_b$ be the velocity of the beam and let U be the velocity of the bow shock, both with respect to the IGM rest frame. Then in the rest frame of the bow shock, the IGM has a velocity of $-U$ and the beam material has a velocity of $V-U$. Thus, the dynamic ram pressure equilibrium is $\varrho_b(V-U)^2\simeq\varrho_m U^2$. Now if we assume the beam material has the pressure P of the IGM (as it does when it enters the grid from the left) we can divide both sides by P. Since the adiabatic index γ is the same on both sides we have the result: $(V-U)^2/C_b^2\simeq U^2/C_m^2$. The strength of a shock can be measured by the Mach number of the flow incident on the shock, e.g. the pressure jump (for $\gamma=5/3$) is $P_s/P_i=\frac{1}{4}(5M^2-1)$, where P_s is the shocked pressure and P_i is the incident pressure. Thus, our simple argument would say that the strength of the Mach disk shock, with incident Mach number M_{v-u}, would equal the strength of the bow shock, with Mach number M_u.

This is *not* what we find. In Fig. 6, we show the pressure contours for the hot ($\varrho_b=0.1$) Mach 3 jet. The pressure jump across the bow shock is 2.1 (each contour line is 1.2 times the previous one), while the pressure jump across the Mach disk is 55. *The Mach disk is a much stronger shock than the bow shock.*

How can one reconcile our numerical results with the simple ram pressure argument? The answer lies in the inherently two-dimensional nature of the flow which results, as described above, in a rarefaction valley before the Mach disk is reached. For the case of Fig. 6, we measure a bow shock velocity $U\simeq 1.6$ or $M_u=1.6$. This compares with the Mach number of the beam gas in the Mach disk rest frame (with $V=3\,10^{1/2}=9.5$) of $M_{v-u}=2.5$, so the dimensional ram pressures are indeed comparable. However from Fig. 6 it is clear that the pressure is *not* constant along the beam, but rather decreases in the rarefaction valley. This pressure decrease is accompanied by a corresponding decrease in the sound speed and an increase in the beam velocity, so that the local Mach number of the pre-shock flow is much higher than 2.5; in fact $M_{v-u}=5.9$. Thus the jump in pressure across the Mach disk exceeds the bow shock pressure jump by the amount of pressure drop along the rarefaction valley.

b) Stability

A comparison of Figs. 4a–c and 5 shows that the geometry of the working surface is not steady. The peculiar indented nose of the jet in Fig. 5 is suggestive of the onset of Rayleigh-Taylor (RT) instability. However, since the jet gas is less dense than the medium gas, the instability may grow only if the working surface is *accelerating*; for instance if the beam luminosity were suddenly increased. But the working surface experiences a secular *deceleration* as it travels further from the source, because of attenuation of the beam luminosity through shocks and surface instabilities. Therefore we expect the contact discontinuity at the head of the jet to be RT stable, and another explanation for the indented feature must be found. Considering the feature as an off-axis protrusion, rather than an on-axis intrusion, then the protrusion's origin is readily understood.

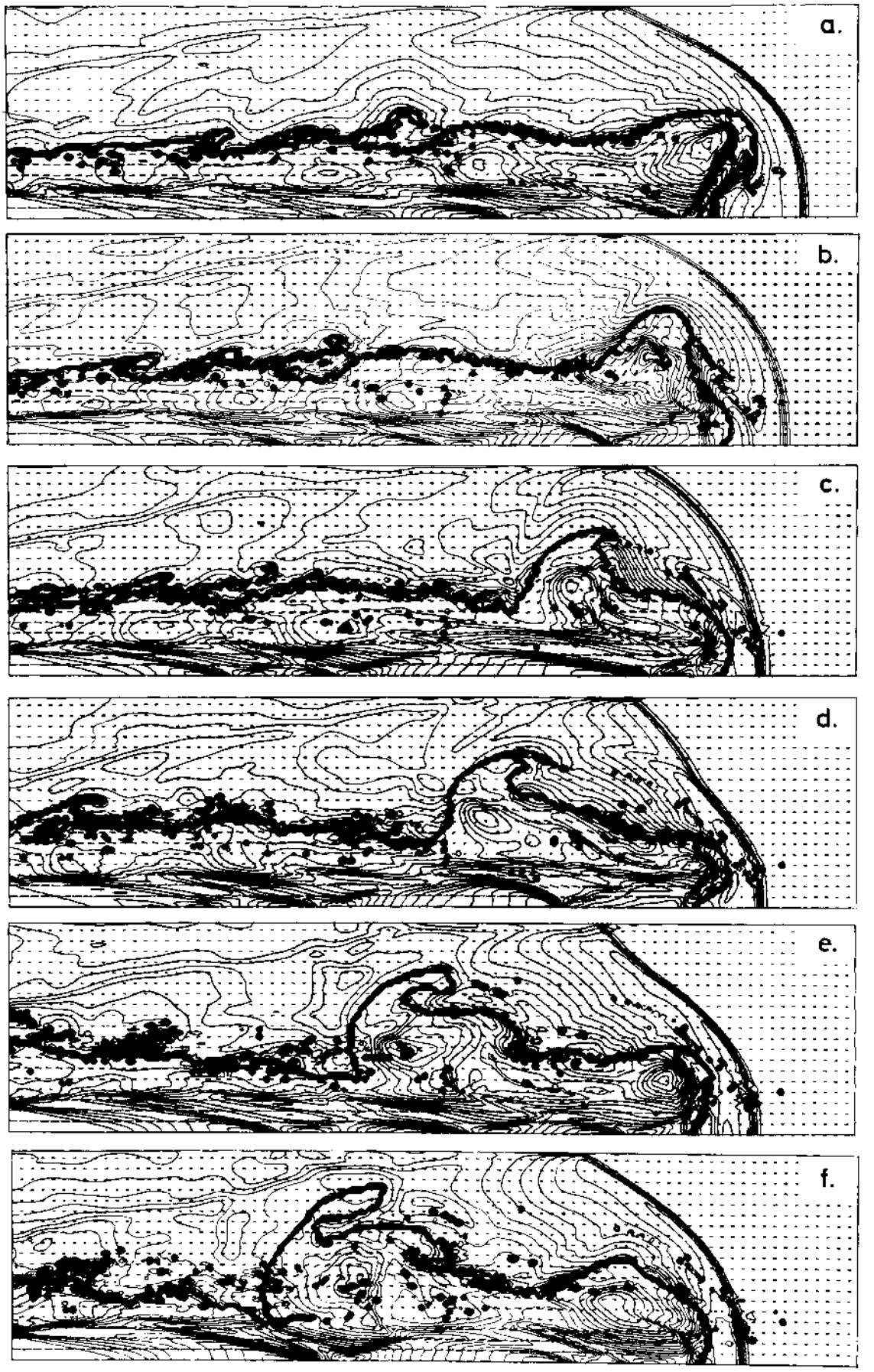
Beam gas passing through the incident and reflected shocks is decelerated less than beam gas passing through the Mach disk. This fact is responsible for the ever-present slip line emanating from a shock triple point. Referring to Fig. 5, we suggest that it is the ram pressure of this gas, flowing above the slipline, that pushes the contact discontinuity outwards.

Regardless of the protrusion's origin, it is a perturbation of a surface that is generally in a state of shear, and must therefore evolve as a *shear wave*. If the contact is subsonically sheared, then the wave grows via the Kelvin-Helmholtz (KH) instability. If the contact is supersonically sheared, then the perturbation damps. In either case the perturbation is advected down the jet, away from the working surface. In order to study this process, we took the Mach 6 jet shown in Fig. 5 and added to all velocities a backward velocity equal to the velocity of the bow shock in the IGM rest frame. By thus transforming to the rest frame of the bow shock we can study the long time stability of the working surface. Figure 7a–f shows a time sequence of this calculation.

As the perturbation grows in amplitude, Fig. 7a–c, it is advected down the jet. Although the perturbation is introduced with a wavelength of the jet diameter, higher wavenumber modes appear as the wave breaks. The process repeats itself in Figs. 7d–f,

© European Southern Observatory • Provided by the NASA Astrophysics Data System

1982A&A...113..285N



© European Southern Observatory • Provided by the NASA Astrophysics Data System

1982A&A...113..285N

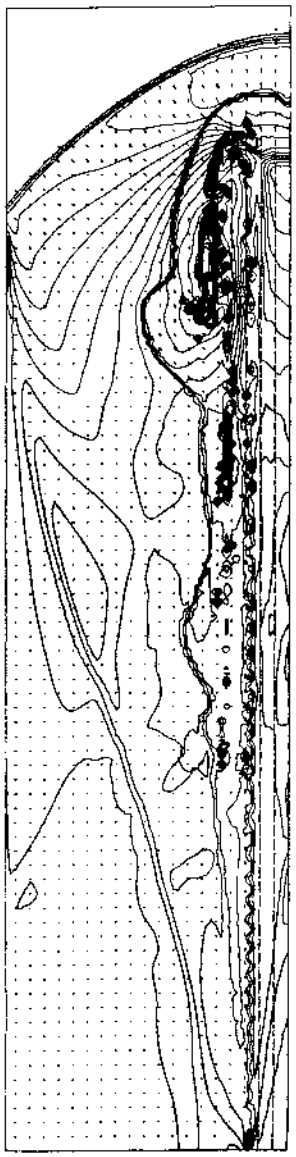


Fig. 8. Density contours and velocity vectors of vortex shedding in a cold ($\varrho_b=1$), Mach 6 jet. Characteristic wavelength is ~ 1.4 jet diameters, as for the hot jet in Fig. 7

although the wave has smaller amplitude. We call this process "vortex shedding" because beneath each wave crest is a low-pressure eye around which the cocoon gas circulates; the vorticity having been generated at the triple shock configuration. Further time integration reveals that vortex sheeding continues in a quasi-periodic manner with a period $t_{vs}\sim 2.8$ and wavelength $\lambda_{vs}\sim 7.8$ for the Mach 6 jet.

Vortex shedding may rely on a feedback mechanism between working surface, cocoon, and beam that involves both the Rayleigh-Taylor and Kelvin-Helmholtz instabilities. Above we argued that the working surface is RT stable. However, KH instabilities of the cocoon boundary may change the sense of acceleration of the working surface by modulating the beam luminosity. Perturbations in the cocoon are transmitted to the beam, which responds by forming internal shock waves (cf. Sect. VII). These shocks can be seen in Fig. 7 beneath each wave crest. Changes in shock strength and position may increase the effective beam luminosity at the working surface, driving a RT instability. The surface deformation produced by the growth of this instability would at the same time propagate back along the jet as a shear wave, perturbing the cocoon, thus closing the feedback loop. Further study of the complicated dynamics at the head of the jet is needed before this mechanism can be verified.

c) Effects of Varying Parameters

Recall from Sect. II that once we have restricted our study to pressure-matched $K=1$ jets, the problem parameters are the beam Mach number M_b, and the beam density ratio ϱ_b. The beam luminosity becomes $L_b=\pi R_b^2 M_b^3/\varrho_b^{1/2}$, indicating that phenomena sensitive to the beam luminosity will be very sensitive to the Mach number, and quite insensitive to the density ratio. We find this to be true in the case of the vortex-shedding phenomenon.

To illustrate the effect of changing the density ratio Fig. 8 shows vortex-shedding in a Mach 6, $\varrho_b=1.0$ jet. Comparing the wavelength of the shed vortices with those in Fig. 7f, one finds they are essentially identical, despite a factor of 10 change in the beam density. This is not surprising considering the perturbation wavelength is set by the diameter of the jet, and that the density ratio enters into the growth-rate of Kelvin-Helmholtz instabilities with only a fractional power.

The beam Mach number has a more substantial effect on the vortex-shedding phenomenon. Generally speaking, lower Mach numbers produce larger vortices. This follows from the observation that at lower Mach numbers ($M_b\lesssim 3$, say), the shocked beam gas accumulates in the vicinity of the working surface, rather than continuously feeding a cocoon. The reason for this is discussed in Sect. VI. This effect is illustrated in Fig. 9, which shows two stages of vortex-shedding in a Mach 3, $\varrho_b=0.1$ jet. In Fig. 9a, the increase in jet diameter towards the working surface indicates gas accumulation in what may better be described as a lobe. In Fig. 9b the lobe has further inflated and is in the process of being shed through the action of surface instabilities. Meanwhile, a new smaller vortex begins to grow near the beam cap. Presumably, this too will inflate and be shed as the jet propagates onward, although this has not been computed.

At lower beam Mach numbers ($M_b\lesssim 1.5$) the activity at the end of the jet is best described as the gradual inflation of a single, slowly moving lobe, rather than the quasi-periodic vortex-shedding found at higher Mach numbers. The beam density ratio ϱ_b has a pronounced effect on the way this proceeds. Figure 10 shows a comparison of two Mach 1.5 jets; one with $\varrho_b=0.1$, and the second with $\varrho_b=1.0$. In the first case (Fig. 10a) the lobe inflates with only minor mixing with the medium gas via short wavelength Kelvin-

Fig. 7. Density contours and velocity vectors of quasi-periodic vortex-shedding at the head of a hot ($\varrho_b=0.1$), Mach 6 jet. The jet pictured in Fig. 5 serves as the initial condition for this calculation in the rest frame of the bow shock. Waves are generated by the Rayleigh-Taylor instability of the contact discontinuity at the head of the jet, and grow by the Kelvin-Helmholtz instability. Characteristic wavelength is ~ 1.4 jet diameters

© European Southern Observatory • Provided by the NASA Astrophysics Data System

1982A&A...113..285N

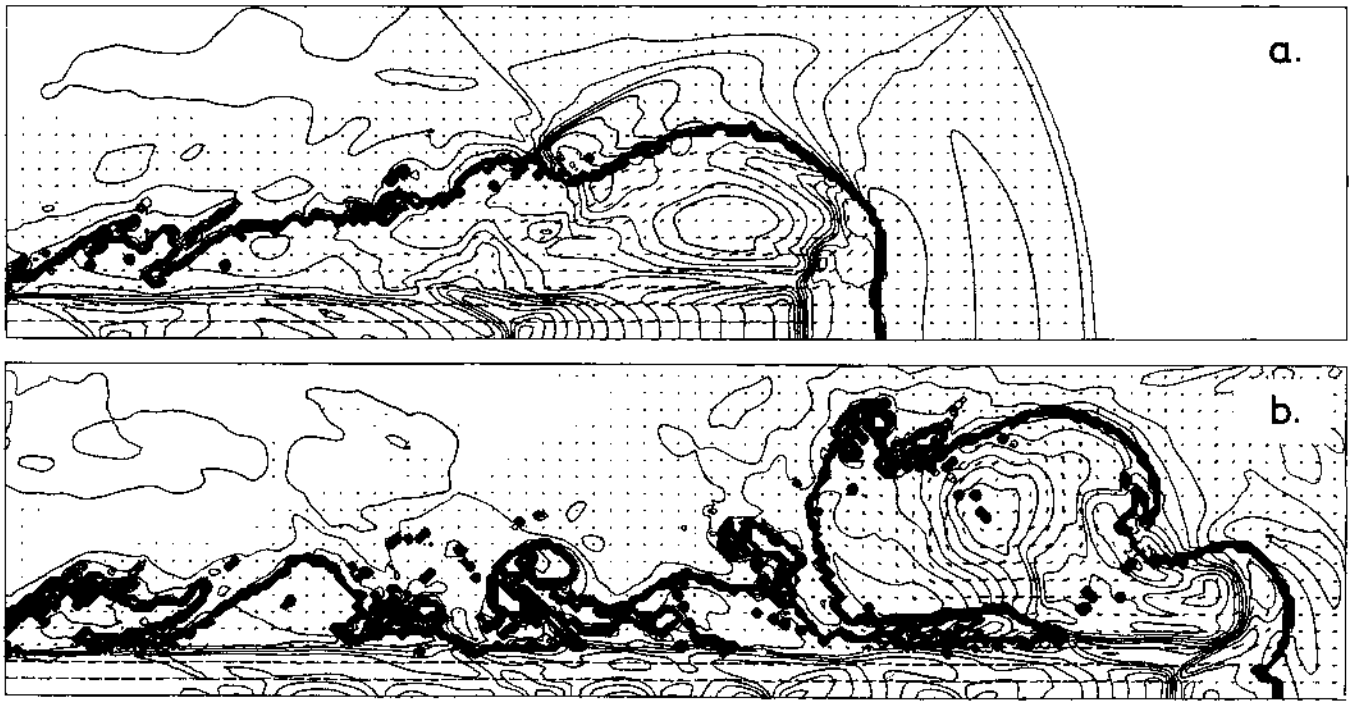


Fig. 9a and b. Structure and stability of a hot ($\varrho_b = 0.1$), Mach 3 jet. **a** Tapered cocoon at lower Mach numbers is due to weaker backflow from the working surface. A well-developed low-pressure "eye" causes the characteristic underexpanded shock configuration at the working surface. **b** Vortex shedding and the disruption of the cocoon via the Kelvin-Helmholtz instability. Notice how intruding "fingers" of IGM are deflected by the beam, and the internal shocks that result. Again density contours and velocity vectors are presented

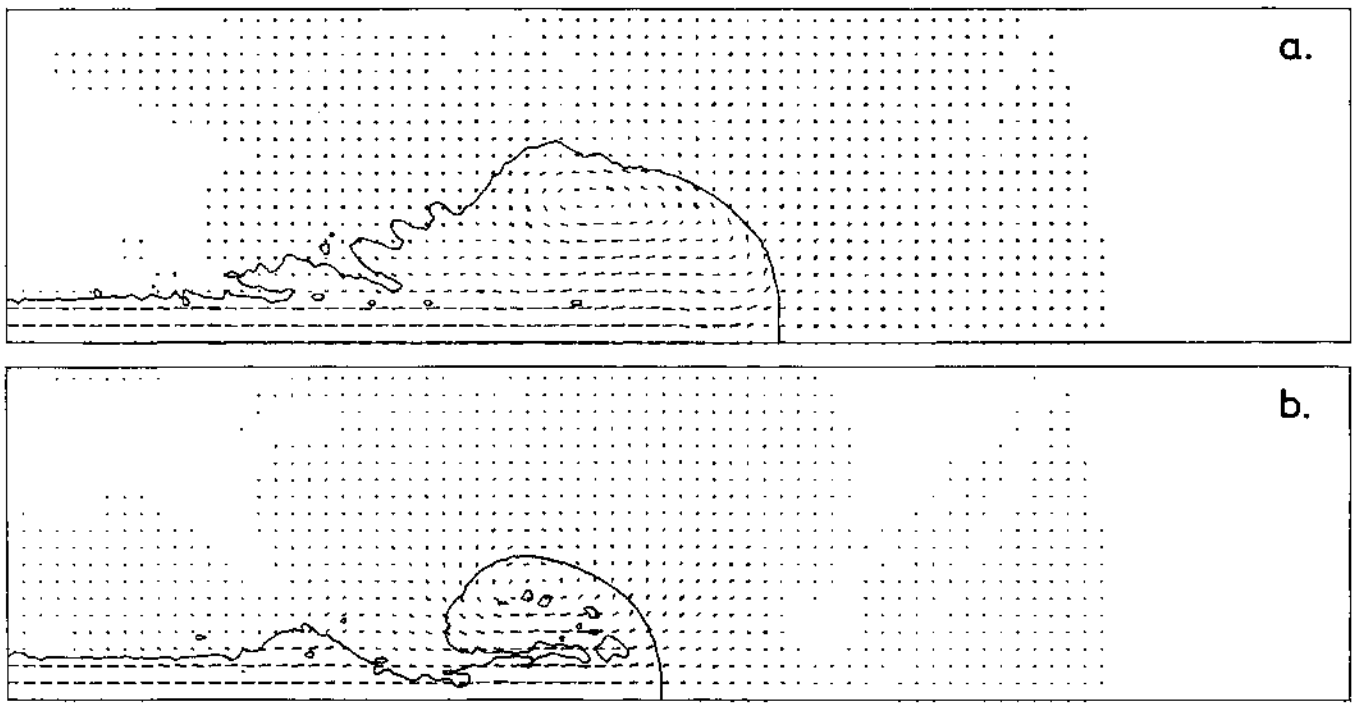


Fig. 10a and b. Comparison of two Mach 1.5 jets, showing the contact discontinuity between cocoon and IGM and velocity vectors, **a** $\varrho_b = 0.1$ case; since $C_b = \sqrt{10}\, C_m$, interior vortical motion is rather decoupled from the flow exterior to the contact discontinuity. **b** $\varrho_b = 1.0$ case; since $C_b = C_m$, medium gas participates in vortical motion, resulting in efficient entrainment at the working surface

© European Southern Observatory • Provided by the NASA Astrophysics Data System

1982A&A...113..285N

Helmholtz modes growing on its downstream side. However in the second case (Fig. 10b) because the sound speeds are equal in and outside the jet, the medium gas participates in the lobe's vortical motion through a kind of mechanical "impedance matching". Medium gas is entrained in the lobe, and the familiar "mushroom cap" geometry results.

VI. Cocoon

The cocoon is supplied by a backflow of beam gas that has passed through the shock configuration at the head of the jet. The strength of the backflow, and therefore the structure of the cocoon, depend strongly on the beam parameters M_b and ϱ_b – the Mach number and density ratio. In this section we summarize cocoon morphology for the 5 cases listed in Table 1, and attempt to explain the morphological differences through a simple analysis of the mechanics of the backflow. We then discuss the role of Kelvin-Helmholtz instabilities on the long-term evolution of the cocoon.

a) Morphology

Consider first the sequence of "hot jets" - $\varrho_b=0.1$; $M_b=6$, 3, 1.5. At Mach 6, the cocoon is very nearly of uniform thickness as a function of distance down the jet, (cf., Fig. 5). The cocoon is fed by a strong backflow which is *supersonic* in the IGM rest frame. In fact the entire cocoon in Fig. 5 is flowing to the left supersonically, a fact that has important implication for the stability of the cocoon. At Mach 1.5, on the other hand, the backflow is *subsonic* in the working surface rest frame, and therefore insufficient to support an extensive cocoon. Rather, the shocked beam gas accumulates in a slowly-filling lobe that moves forward with the velocity of the working surface. Away from the lobe the beam is without cocoon in direct contact with the IGM, as can be seen in Fig. 10a. The Mach 3 jet shown in Fig. 9a is clearly an intermediate case. The backflow is supersonic above the low-pressure eye, but then turns subsonic and in certain regions even turns back towards the head of the jet.

We now turn to the sequence of "cold jets" – $\varrho_b=1.0$; $M_b=6$, 1.5. Figure 8 gives a false impression that at Mach 6, the cocoon is established in much the same way as in the $\varrho_b=0.1$ case, i.e. through a strong backflow. In fact the backflow is minimal[2]. Cocoon gas is found to be nearly at rest in the IGM rest frame. We observe that as the jet advances, gas in the beam cap basically moves aside and is left behind. The somewhat uniform thickness of the cocoon is more a result of the high speed at which the cocoon is "laid down", rather than redistribution via backflow. At Mach 1.5, backflow is small even in the rest frame of the working surface and, as in the $\varrho_b=0.1$ case, cocoon gas is confined to a lobe that inflates as it moves forward with the velocity of the working surface (cf. Fig. 10b).

Thus, we find that low Mach number jets ($M_b \lesssim 1.5$) have no cocoon, but only lobes in the vicinity of the working surface. Intermediate Mach number jets ($M_b \approx 3$) may have segments without a cocoon, or at least a messy cocoon in the process of mixing with the IGM via Kelvin-Helmholtz instabilities. Only in the case of high Mach number jets ($M_b \geqq 6$), do we find extensive cocoons, particularly so in the case of hot jets ($C_b > C_m$).

2 Here we mean backflow with respect to the IGM restframe. In the restframe of the working surface there is backflow, but not nearly as strong as in $\varrho_b=0.1$, $M_b=6$ case

b) Backflow Mechanics

We have described how differences in cocoon morphology are related to the strength of *backflow* coming from the working surface. Here we present qualitative arguments that relate the strength of the backflow to the beam parameters M_b and ϱ_b. We begin by examining in more detail the flow in the vicinity of the beam cap.

In the rest frame of the working surface, we know from the symmetry of the situation that the tip of the jet is a stagnation point. Therefore, by the Bernoulli theorem the thermodynamic pressure is a maximum there, both inside and outside the jet. It follows that both internal and external flows will be directed away from this point to regions of lower total pressure (thermodynamic + ram), provided they exist. In the neighborhood of the stagnation point, the flow is transverse to the beam because there is no transverse component of the ram pressure, whereas the thermodynamic plus longitudinal component of the ram pressures of the beam and post bow-shock IGM exactly balance the thermodynamic pressure in the beam cap. Beyond the radius of the beam, the ram pressure of the incoming IGM is not balanced by the beam ram pressure, thus the flow turns back along the direction of the beam.

Far from the working surface, the jet and IGM are in pressure equilibrium at the ambient pressure $P_m=\gamma^{-1}\varrho_m C_m^2$. The jet may be simply the beam, or beam surrounded by a cocoon. If the jet includes an extensive cocoon, then far from the working surface the cocoon must also be in pressure equilibrium with the beam and IGM, with pressure P_m. Denote the pressure in the beam cap P_{bc}. The cocoon is sustained by gas flowing from the beam cap back along the beam (for the mechanical reason just given) by virtue of the pressure difference $P_{bc}-P_m$. Now, since $P_{bc} \propto M_b^2 \cdot P_m$, we see that only for M_b significantly greater than 1 will extensive cocoons be formed and sustained. A high pressure difference may drive a supersonic backflow whose kinetic energy is not quickly dissipated in the vicinity of the working surface by Kelvin-Helmholtz instabilities. This is the case in the $M_b=6$, $\varrho_b=0.1$ jet. At low Mach numbers ($M_b<3$), $P_{bc}-P_m$ is not great enough to drive supersonic backflow, and the combination of a small backflow velocity and flow dissipation via Kelvin-Helmholtz instabilities serves to keep the cocoon gas nearby the working surface in the form of a lobe.

The beam Mach number M_b is not the only parameter determining the strength of the backflow, for in the $M_b=6$, $\varrho_b=1$ case very little backflow (in the IGM restframe) is found. This is understood as the effect of inertia by writing the Bernoulli equation for a streamline passing from the beam cap into the cocoon:

$$\tfrac{1}{2} V_{bc}^2 - \tfrac{1}{2} V_{\text{cocoon}}^2 = -(\gamma/\gamma - 1)(P_{bc}-P_m)/\varrho_b.$$

Here we have made the approximation that differences between ϱ_{bc}, ϱ_{cocoon}, and ϱ_b are small compared to ϱ_b. The change in V^2 is 10 times smaller in the $\varrho_b=1$ case as in the $\varrho_b=0.1$ case, since the pressure difference $P_{bc}-P_m$ is unchanged. Thus backflow is maximized in hot, high Mach number jets.

c) Stability

The cocoon gas generally moves with the speed neither of the beam nor of the external medium, implying the existence of a *vortex sheet* at its inner and outer boundaries. The stability of the vortex sheet between cocoon and beam largely determines the collimation and propagation characteristics of the beam. This topic will be discussed in Sect. VII. The stability of the vortex sheet between

© European Southern Observatory • Provided by the NASA Astrophysics Data System

1982A&A...113..285N

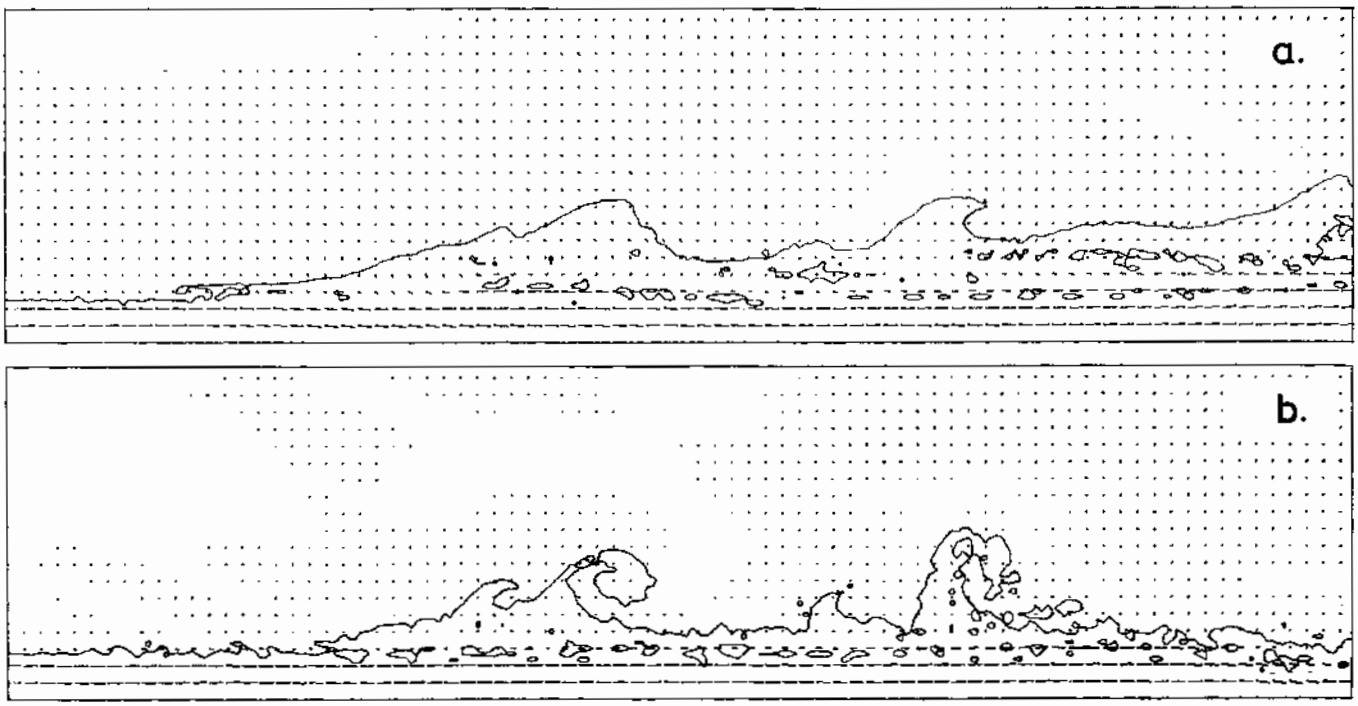


Fig. 11. Vortex sheet "roll-up" of the perturbations on the cocoon of the cold ($\varrho_b = 1$), Mach 6 jet seen in Fig. 8. Cocoon/IGM-interface and velocity vectors are displayed

cocoon and IGM determines how the cocoon evolves as a component of the jet, particularly with regard to entrainment of the external gas. There is currently a growing body of literature in the linear stability of a vortex sheet, particularly in cylindrical geometry (Ferrari et al., 1978, 1980, 1981; Ferrari et al., 1982). However an essential result remains unchanged from earlier investigations (Gerwin, 1968 and references therein): the vortex sheet is stable to linear perturbations for sufficiently high relative Mach numbers. Our calculations suggest that the outer vortex sheet may be stable for sufficiently high Mach number ($M_b \gtrsim 10.$) sufficiently hot ($\varrho_b \lesssim 0.1$) jets because of supersonic backflow in the cocoon. Our computed jets, however, (cf. Table 1) lie in the unstable or marginal regime. Here we summarize the effects of instability growth to nonlinear amplitudes on the cocoon, or lobe as the case may be.

The $M_b = 6$, $\varrho_b = 0.1$ jet seems to have a marginally stable outer boundary. Figure 4a–c show that the cocoon/IGM interface maintains a rather undistributed appearance, except for a noticeable wave about 3 jet radii from the end (cf. Fig. 4c). Closer study reveals that the cocoon is moving supersonically to the left with respect to the IGM, except for directly under the wave, where it is subsonic. Apparently the cocoon was perturbed with a large enough amplitude to set up flow conditions that allowed perturbation growth, i.e. the perturbation induced a locally subsonic velocity-of-shear at the outer vortex sheet. We find subsonic zones in the cocoon moving with the waves displayed in Fig. 7, as well. A mechanism that produces large perturbations has been suggested in Sect. Vb. A result of nonlinear instability growth evident in Fig. 7f is chunks breaking off of the cocoon that remain surrounding the jet.

Figure 4d–f show instability growth arising when the cocoon flow becomes wholly subsonic with respect to the external medium. In the computation this is artificially induced by allowing the working surface to leave the computational domain, thus eliminating the source of the supersonic backflow. While occurring prematurely in our simulation, we expect that sufficiently far from the head of the jet the cocoon backflow will decelerate as shown in Fig. 4d–f. The mixing will not be complete, resulting in an inhomogeneous cocoon.

The diagonal compression wave seen advancing in Fig. 4d–f, and labelled "pressure wave" in Fig. 5 is an artifact of the calculation, and is though not to be important in the discussion of cocoon stability. This and other numerical effects are discussed in the appendix.

Because of the absence of supersonic backflow in the cocoon, the $M_b = 6$, $\varrho_b = 1$ jet possesses a wholly unstable outer boundary. The perturbations evident in Fig. 8 rapidly "roll up" in the sequence in Fig. 11. Chunks of cocoon remain surrounding the jet. An explanation for the nearequality of perturbation wavelength between Fig. 11 and Fig. 7f has been proposed in Sect. Vb as resulting from a characteristic instability at the working surface.

The remaining 3 cases also lack supersonic backflow in the cocoon (lobe) and therefore possess unstable outer boundaries. Figure 9 graphically displays, in the case of a $M_b = 3$, $\varrho_b = 0.1$ jet, how Kelvin-Helmholtz and Rayleigh-Taylor instabilities generally appear together in the nonlinear regime. Beginning as a small amplitude KH mode in Fig. 9a, it develops into the RT "finger" thrusting in under the vortex at the head of the jet in Fig. 9b. Elsewhere along the jet, slender RT fingers displace the cocoon and perturb the beam itself. The fingers are broken by RT instability if accelerated by the light cocoon gas. The mixing of the IGM with the lobe and cocoon thus proceeds by a complicated superposition of the two basic flow instabilities.

Figure 10a shows the growth of short wavelength KH instabilities on the lobe of the $M_b = 1.5$, $\varrho_b = 0.1$ jet. As the lobe fills and moves forward, instabilities break chunks off its rearward side

© European Southern Observatory • Provided by the NASA Astrophysics Data System

1982A&A...113..285N

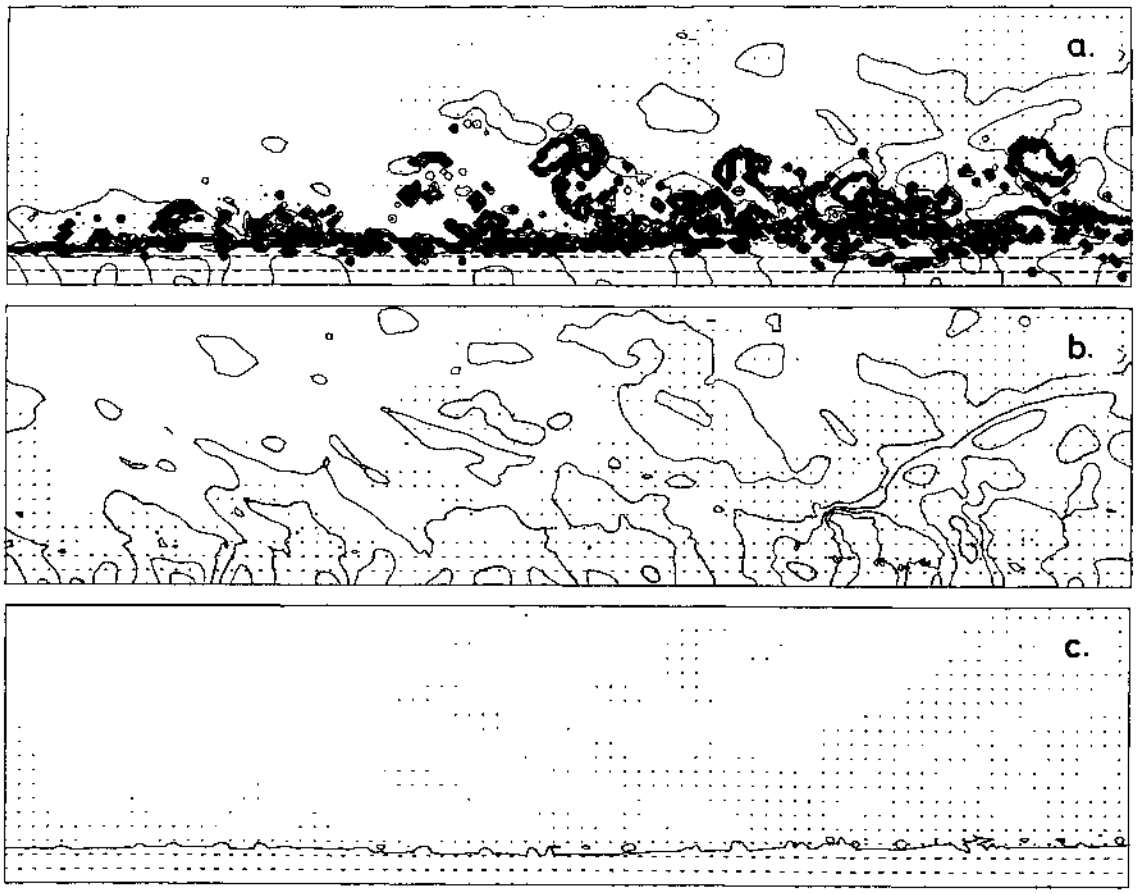


Fig. 12a–c. Quasi-stationary jet structure of the $\varrho_b = 0.1$ $M_b = 1.5$ case at $t = 60$ (8 sound crossing times the short way). **a** Density-velocity plot showing jet debris from lobe instabilities. **b** Pressure-momentum plot showing relative absence of internal structure. **c** Mach number – Mach vector plot. The contour line separates subsonic and supersonic flow; the vectors have length proportional to the local Mach number, and direction of the flow. Beam divergence is 1 zone out of 240. Flow direction is from left to right

that remain behind in a trail (Fig. 12a). Very little IGM gas is entrained in the lobe, however. At $M_b = 1.5$, $\varrho_b = 1$ though, the IGM swirls into the lobe (Fig. 10b), and is thereby entrained.

VII. Beam

The beam is the central energy-carrying channel of the jet. We have left the discussion of beam structure and stability to last because of the need to first understand the environment through which the beam must propagate. The beam environment is either a cocoon (or lobe) in various states of motion and mixing with the IGM, or simply unmixed IGM gas depending, in general, on the beam parameters and position along the jet. We can now consider the structure and stability of the beam itself.

a) Structure

A major feature discovered here is the ubiquity of internal shock waves in supersonic beams. In Fig. 13, we show both a Mach 3 and a Mach 6 hot ($\varrho_b = 0.1$) jet at late times. Any pressure perturbation at the surface of the beam will cause an oblique shock. The pressure perturbation travels inward at the sound speed C_b, but is swept downstream at $V_b = M_b C_b$. One can see that the Mach 3 jet is about twice as steep as the Mach 6 jet in agreement with this simple argument. The spacing of the resulting alternate high and low pressure features along the jet seems to be roughly independent of the Mach number, and equal in distance to the jet diameter. We interpret this as evidence that the perturbations are caused by Kelvin-Helmholtz instabilities of the cocoon/IGM vortex sheet at the dominant wavelength rather than KH instabilities of the beam/cocoon vortex sheet itself. Below we will argue that the latter surface is stable. Supporting evidence is presented in Fig. 13a, which clearly shows a shockwave being touched off by a dense finger of IGM gas that has penetrated the cocoon.

An important property of oblique shock waves is that they *collimate* the beam: gas is turned towards the jet-axis upon passing through the shock. This is simply a statement that the shock originates from an inward compression of the beam. However, oblique shock waves would still be produced by a sudden expansion of the beam, as in the case of an underexpanded jet, described in Sect. III. Thus, in either case, one or several oblique shock waves will keep the beam flowing parallel to its axis.

Globally, rich shock structure is found near the head of the jet where Kelvin-Helmholtz instabilities in the cocoon/lobe first grow to large amplitude. Further back along the jet, less shock structure is evident as in Fig. 12b, where the perturbing motions have settled

© European Southern Observatory • Provided by the NASA Astrophysics Data System

1982A&A...113..285N

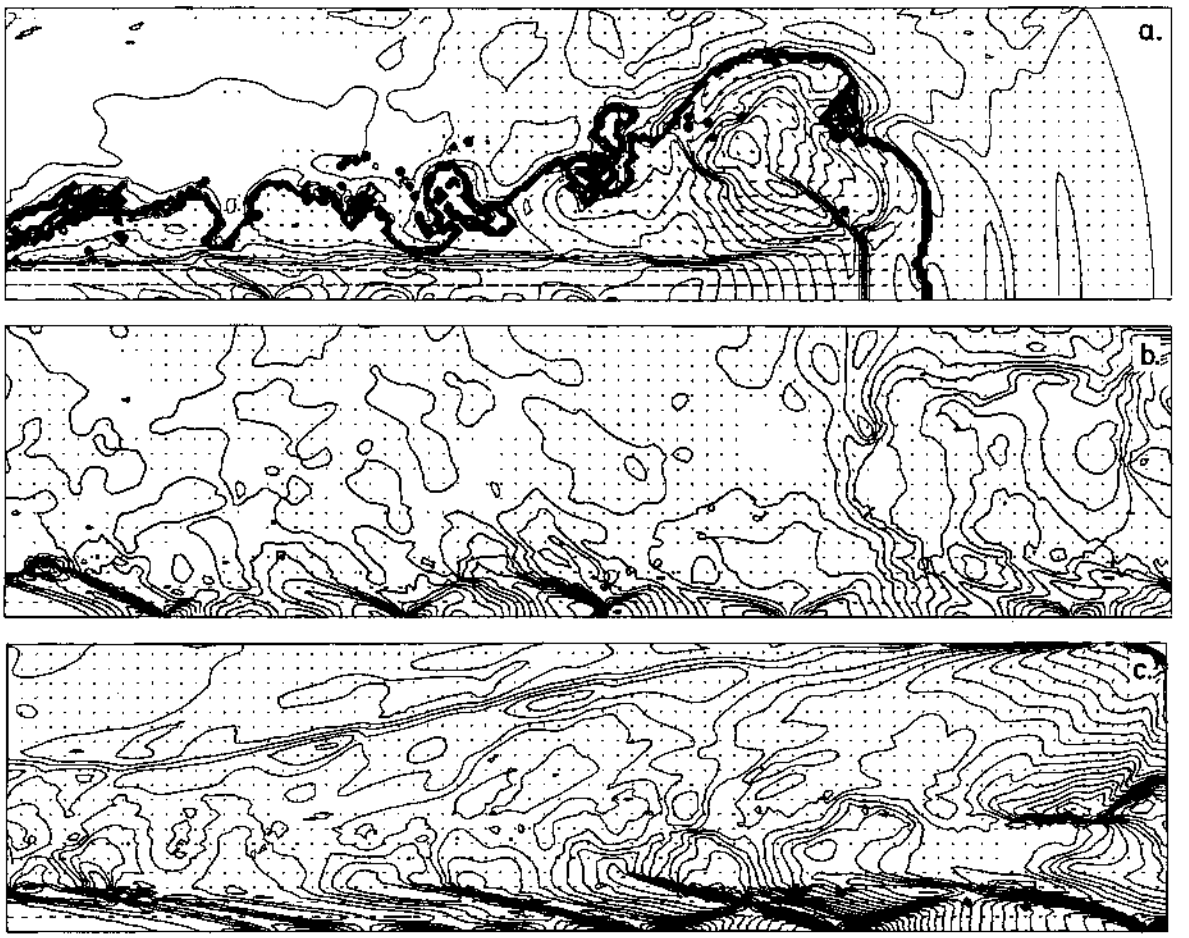


Fig. 13a–c. The origin and nature of internal shockwaves. **a** Density contours showing how instabilities on the cocoon boundary of a hot ($\varrho_b = 0.1$), Mach 3 jet excite oblique shockwaves in the beam when fingers of dense IGM gas touch the beam (left). **b** Pressure contours of a Mach 3 jet reveal quite regular shock spacing. **c** Pressure contours of a Much 6 jet show shock spacing is quite insensitive to the beam Mach number, but rather depends on the diameter of the jet

down. Shown is a Mach 1.5, hot ($\varrho_b = 0.1$) beam that meets the IGM at a stable interface.

Beam collimation, as judged by the opening angle of the boundary between supersonic and subsonic flow, is surprisingly good. Figure 12c shows this boundary at $t = 60$, or 8 sound-travel times between the beam and the pressure boundary. The deviation of the boundary from parallel is only 1 zone out of 240 – the limit of our computational resolution.

b) Stability

The beam meets cocoon, lobe, or the IGM at a vortex sheet. The stability of this surface determines whether the beam can propagate a great distance from its source, and is currently one of the central issues in the study of galactic radio jets. Our calculations show, subject to the qualifications set forth in the appendix, that the hot ($\varrho_b = 0.1$) beams are stable for Mach numbers as low as 1.5. Despite large perturbations applied over extensive portions of the Mach 3 and Mach 6 beams due to cocoon instabilities (cf. Figs. 4, 7, and 9b), the beams are not disrupted. The Mach 1.5 beam is in direct contact with the IGM, and maintains remarkable collimation (cf. Fig. 12). The cold ($\varrho_b = 1$) Mach 6 beam is also found to be stable to disruptive KH modes (cf. Fig. 11). Stability in these cases imply high propagation efficiency and negligible entrainment of IGM gas by the beam.

We studied the long-term dynamics of a cold ($\varrho_b = 1.0$), $M_b = 1.5$ jet as a worst possible case for beam disruption to Kelvin-Helmholtz instabilities. Like the hot $M_b = 1.5$ jet, the beam is in direct contact with the IGM. Unlike the hot $M_b = 1.5$ jet, the beam is unstable. Figure 14 shows a time sequence of the beam interface, and gives some insight into the nonlinear phase of the Kelvin-Helmholtz instability in slender, axisymmetric beams. The characteristic wavelength of the instability is seen to be roughly twice the beam diameter consistent with predictions made on the basic of linear theory (Ferrari et al., 1981). Most noticeable is the asymmetry between the shapes of the inward and outward extending parts of the wave. We see in Fig. 14a that the inward extending part of the wave extends over a smaller fraction of a wavelength than the outer extending part of the wave. As the wave grows (Figs. 14b–e), the inward extending parts are swept further inward and along with the flow. The characteristic cavity/nozzle geometry is thus established. The flow is supersonic in the cavity and subsonic in the nozzle; the deceleration being affected by a shock standing just upstream of the nozzle. Thus, internal shock waves are a structural characteristic of unstable beams as well. The walls of the nozzle are

© European Southern Observatory • Provided by the NASA Astrophysics Data System

1982A&A...113..285N

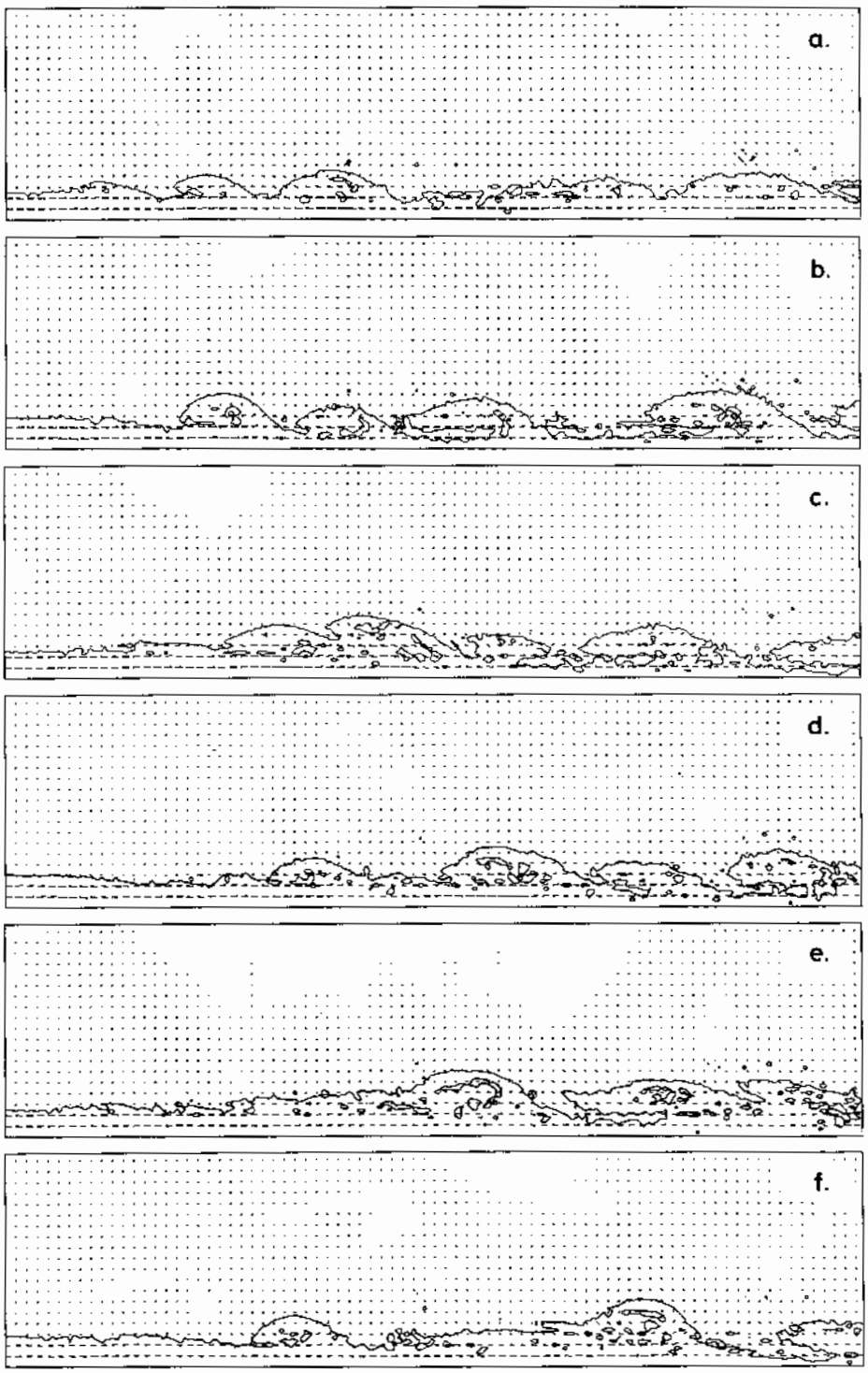


Fig. 14a–f. Kelvin-Helmholtz instabilities of the boundary (solid line) of a cold ($\varrho_b = 1$), Mach 1.5 beam. **a** and **b** Nonlinear growth of modes producing characteristic cavity/nozzle geometry. Supersonic flow in each cavity is decelerated to subsonic flow in each nozzle by a compression wave or a shock front. **c–f** Breakup of nozzles efficiently entrains the external medium gas. Dominant KH wavelength ~2.1 beam diameters

thin and break into pieces via the Rayleigh-Taylor instability. In this way, a Kelvin-Helmholtz unstable beam entrains IGM gas quite efficiently.

Is the beam disrupted? Since our analysis is limited to axisymmetry, the dissipation of beam luminosity through surface instabilities and entrainment is the only form of beam disruption accessible. In this sense the beam is disrupted. Nevertheless, the beam will continue to propagate until it becomes wholly subsonic, whereupon it will mix with the IGM.

VIII. Summary and Astrophysical Implications

The structure and stability of the basic jet components conceived by Blandford and Rees (1974) – beam, working surface, and cocoon – have been studied for various beam Mach numbers and density (and therefore temperature) ratios. We find that supersonic beams of collimated gas in pressure equilibrium with the intergalactic medium propagate efficiently at high Mach numbers ($M_b \geq 6$, say). At the working surface, the beam is decelerated by a

© European Southern Observatory • Provided by the NASA Astrophysics Data System

1982A&A...113..285N

Mach-disk shock front which is in general much stronger than the bow shock running ahead of the jet. Backflow from the working surface will support an extensive cocoon surrounding the beam provided the beam temperature considerably exceeds the confining gas temperature ($T_b \geqq 10\, T_{\rm IGM}$, say). For sufficiently "hot" high Mach number jets, the cocoon backflow is supersonic, raising the possibility of a wholly stable supersonic jet. At low Mach numbers and temperature ratios, the backflow is less strong, producing lobes instead of cocoons. These lobes and low-velocity cocoons are generally unstable to the Kelvin-Helmholtz instability, leading to a very ragged outer jet boundary as the two gases mix. The dominant wavelength of this instability is approximately 1–2 jet diameters; the original perturbations deriving from nonsteady but quasi-periodic behaviour at the working surface that we call vortex shedding.

Waves and instabilities on the cocoon/IGM boundary generally perturb the beam, which is itself stable except in the very lowest Mach number ($M_b = 1.5$), lowest density ratio ($\varrho_b = 1.0$) case. Perturbations set up internal shock waves in the beam which are spatially quasi-periodic because the perturbation is spatially quasi-periodic. Thus the shock spacing is generally 1–2 jet diameters, fairly independent of the beam Mach number. If the beam boundary itself is Kelvin-Helmholtz unstable, shocks and compression waves internal to the beam are also found to have a quite regular spacing of ~ 2 beam diameters. We conclude that quasi-periodic internal shocks will exist in regions of a supersonic jet undergoing global and therefore disruptive Kelvin-Helmholtz instabilities.

The abundance of internal shocks in regions of global instability suggest that if, as proposed by Blandford and Ostriker (1978), shock fronts are the source of relativistic electrons, then these regions should be areas of higher synchrotron emission and lower spectral index. Knots could be understood as emission from the shock fronts themselves, or as emission from the high density regions that occur behind each shock front.

Of course, the strongest shock front in a high luminosity jet, giving the highest post-shock density, occurs at the working surface. Since we have confirmed the structural model of Blandford and Rees' working surface, we judge as sound their explanation of hot spots as synchroton emission from this region. The construction of theoretical radio maps using our detailed structural information plus a model for the synchrotron emission should help elucidate the nature of hot spots. Of particular interest would be to see whether the double hot spots observed in some radio lobes (Miley, 1980) could be understood as a signature of the triple shock configuration found to exist at the working surface.

Finally, by piecing together the results from the different numerical experiments, we suggest the following evolutionary sequence in the life of a hot supersonic jet. Imagine a high luminosity source of hot jet gas turning on and being collimated into a high Mach number beam by some unspecified mechanism operating at the center of an elliptical galaxy. The jet efficiently bores through the interstellar gas and then through intergalactic gas, looking quite similar to the jet in Fig. 5. The efficiency is high because the beam is stable and, due to supersonic backflow from the working surface, the cocoon is stable as well. There may be surface waves on the cocoon stemming from unsteadiness of the working surface geometry. Depending on the amplitude of the surface waves, internal shocks of varying strength are set up in the beam. The working surface contains a very strong shockfront which appears as an intense hot spot.

As the jet becomes longer, cumulative propagation losses decrease the Mach number towards the end of the jet. Backflow from the working surface becomes subsonic with respect to the external gas, and a wave of Kelvin-Helmholtz instability sweeps back along the cocoon. Near the end of the jet the instabilities, and therefore the internal shocks they induce, are the strongest, (cf. Fig. 9b). The previously stable cocoon nearer to the galaxy becomes unstable as a rarefaction wave, which communicates the loss of support from the working surface, sweeps back through the cocoon (cf. Fig. 4d–f). The wealth of internal shocks in the unstable region energize electrons to produce synchrotron emission of increasing intensity as the hot spot is approached, which is now somewhat weaker than before.

Finally, when the cumulative beam losses equal the source kinetic luminosity, the jet reaches its maximum spatial extent. At the working surface the beam itself becomes subsonic and therefore unstable, and terminates in a chaotic flow that feeds a growing radio lobe.

If this model is correct, then the fluid dynamics near and in the lobe would be quite interesting. For example, it is likely that the beam structure entering the radio lobe would be quite complex with internal shocks, which maintain the population of relativistic electrons to light up the radio lobe via synchrotron emission. Magnetic fields that were dynamically unimportant in the beam could be amplified by the vortical motion, and become dynamically important in the lobe. If the lobe pressure (magnetic and thermal) were to increase beyond the beam pressure, then beam choking would occur. The Mach disk at the choke point would assume the function of the working surface, while the working surface at the leading edge of the lobe would rapidly disappear. This may account for the "ghost" hot spot that can be seen in the 21 cm map of DA 240 by Strom and Willis (1981).

According to this model, we would interpret edge-brightened radio doubles as the ends of high luminosity jets still in the process of plowing outward through the intergalactic gas. Edge-darkened radio doubles with inner hot spots would be interpreted as jets that have reached their maximum spatial extent. The inner hot spots would indicate the points where the beam is choked. This could arise at a pressure jump in the confining gas, or more likely, due to a drop in the beam pressure if, for example, the luminosity of the central engine were to decrease.

The largest uncertainty that is not addressed in this paper is the possible disruption of the beam by nonaxisymmetric surface instabilities; the garden hose instability being potentially the most disruptive because it destroys the pointing accuracy of the beam. We must also consider fluting modes of the beam, as well as both the garden hose and fluting modes of the cocoon/IGM boundary. The worrying point is the following: in a shear flow of arbitrarily high relative velocity v, it is always possible to choose a disturbance with wave vector k, such that $v \cdot k/|k|$ is less than the speed of sound of both fluids. Such disturbances will grow via the Kelvin-Helmholtz instability. Although these nonaxisymmetric modes may grow, which ones are capable of disrupting the jet?

We suggest that the cocoon will not develop the garden hose instability until the central beam itself develops the instability, for the cocoon is constrained to follow the trajectory of the beam. Also, even though fluting modes may grow on the boundary of a supersonically backflowing cocoon, thus eliminating the possibility of a stable outer boundary, these modes only induce more internal shock waves in the beam than would be the case in axisymmetry. Thus, the stability of the jet relies on the stability of the beam.

Concerning the beam boundary itself, we suggest that nonaxisymmetric instabilities are unimportant except below some critical Mach number of order unity. Consider an extended jet that

© European Southern Observatory • Provided by the NASA Astrophysics Data System

1982A&A...113..285N

terminates subsonically. The modes that grow on the high Mach number part of the beam make such a small angle with respect to the flow that they remove very little of the beam thrust. Thus we suggest that the majority of the beam is not disrupted despite the existence of surface instabilities. Near the end of the jet, however, the wave fronts make ever larger angles with respect to the beam axis as the Mach number drops, and thereby remove more momentum from the beam. It is likely that the beam will become unstable to the garden hose mode in approximately the range of parameters where we found the axisymmetric instability to grow; that is, as the beam Mach number drops close to unity.

There is some support for this proposal by recent high resolution photographs of the M87 optical jet by Nieto and Lelièvre (1982), as well as the 2 cm radio maps of Owen, Hardee, and Bignell (1980). Nieto and Lelièvre derive a rather regular spacing of knot "complexes" that are aligned with the nucleus and *increase* in intensity, as one moves outward from the nucleus toward knot *A*. At that point, the jet develops a regular wiggle in the alignment of several more knots of *decreasing* intensity. The observationally determined ratio of knot spacing to knot diameter is ~ 2, consistent with our ratio of shock spacing to beam diameter in an unstable beam. A possible interpretation is that the knots we are seeing in M87 are related to shocks in an unstable beam which reach peak strength in the region where global instabilities first set in. Upstream of this region, the shocks (and therefore the knots) are weaker, because, even though Mach numbers are higher, the beam is not strongly perturbed. Downstream of this region, the shocks (and therefore the knots) are weaker because, even though instabilities strongly perturb the beam, they have also decelerated the beam to low Mach numbers ultimately less than unity. Whether the onset of the garden hose instability coincides with the region of peak emission is a point that must await further detailed numerical simulations. In this regard, work is in progress to study odd perturbations across the center-plane of a jet with slabsymmetric geometry in both the nonrelativistic and relativistic regimes. On the basis of linear studies (Ferrari et al., 1982), we expect this to simulate quite effectively the helical and fluting modes of a cylindrical jet.

A final warning must be given concerning the use of the ideal fluid equations in modelling astrophysical jets. MHD and mode coupling effects may be important for the collimation and stability of the flow. In addition, dissipative effects could operate in boundary layers that could introduce new large scale phenomenologies. An even more fundamental issue is whether energy loss through synchrotron radiation is important dynamically. Numerical experiments addressing these issues are planned once ideal jets are well understood.

Acknowledgements. We would like to recognize the contributions of Drs. James M. LeBlanc and James R. Wilson to making the foregoing computations feasible. Their enormous experience in numerical Eulerian hydrodynamics underlies almost every aspect of the code we used. We acknowledge insightful discussions with Drs. R. Breuer, S. Colgate, F. Meyer, and P. Woodward. We gratefully acknowledge the generous support of Prof. R. Kippenhahn, as well as the close cooperation of the staff of the computing center of the Max-Planck-Institut für Plasmaphysik, which allowed us to carry this project through to completion despite a long holiday week. L. S. and M. D. S. wish to acknowledge partial financial support from the National Science Foundation under grant Nos. PHY 80-01496 and PHY 78-04404. Finally, we would like to thank Seymour Cray for building such a good computer.

Appendix: Numerical Effects and Uncertainties

Here we discuss several numerical effects and uncertainties inherent in the calculations and their relative importance to the overall results. In particular we consider the numerical modelling of shear surfaces, and the choice of the flow boundary conditions.

a) Modelling Shear Surfaces

A shear surface, or *vortex-sheet* is a surface across which the tangential component of velocity and perhaps density change in a discontinuous manner. In contrast, a *shear layer* is a region of finite transverse extent across which the above mentioned variables continuously change value. In general the stability properties of these two types of shear flows differ for perturbation wavelengths $\lesssim$ the shear layer thickness. Now, in a real fluid a vortex sheet will always evolve into a shear layer due to the effects of viscosity or some other diffusive process. But we have used the ideal equations in our numerical simulations, and therefore the two vortex sheets in the jet – one between beam and cocoon, and one between cocoon and IGM – should remain vortex sheets, ignoring for the moment Kelvin-Helmholtz instabilities. However truncation errors in the finite difference approximations of the ideal equations introduce a kind of *numerical diffusion* which in general spreads an initial shear surface into a shear layer several computational zones wide. This means that the numerical description and evolution of a shear surface becomes increasingly inaccurate when one considers modes of smaller wavelength (in terms of the number of zones in a wavelength). We might be tempted to say that the numerical diffusion acts in some way as a substitute for the dissipative mechanisms that must occur in a real fluid, however, numerical diffusion, in general, acts neither quantitatively nor qualitatively like the real process. The upshot of these considerations is that sufficient zoning resolution should be taken so that the behavior of shear waves only a few zones in wavelength is unimportant for the gross features of the flow. Equivalently, features of only a few zones in extent should not be taken seriously.

In our jet similations, we are concerned with disruptive instabilities; that is, shear surface instabilities with a wavelength comparable to the jet or beam diameter. Therefore given a sufficient number of zones across the beam and jet, then potentially disruptive shear waves on the beam and jet boundaries will be accurately modelled. How many zones is a sufficient number? That depends on the accuracy of the numerical method, but for our approach a conservative estimate is 20 zones per wavelength. On this basis, the unstable beam in Fig. 14 is adequately resolved; there are typically 30–40 zones per wavelength. Likewise, vortex-shedding in Fig. 7 is well resolved; having typically 30 zones in a half-wavelength. The finer-scale aspects of shear wave evolution should be given weight according to the number of zones in the feature: thus, for example, the single-zone "black-dots" seen in all calculations involving unstable interfaces are not to be believed, however the chunks of lobe gas in Fig. 10a have 20 zones in each, and can be believed.

In Sect. VII, we concluded that the beams were all stable except for the $\varrho_b = 1$, $M_b = 1.5$ case. It might be argued that microinstabilities may exist at the edge of the beam, that we are not resolving, which build a shear layer of increasing thickness that would change the large scale stability of the beam. However it is expected that the mixing angle of a supersonic shear layer would be very small, thus

© European Southern Observatory • Provided by the NASA Astrophysics Data System

1982A&A...113..285N

confining the microinstabilities to a layer of small thickness (compared to the beam) if they began there.

Preliminary calculations on a supersonic shear layer by LeBlanc (private communications) confirm this, for he observes that whenever a "finger" of matter from the unstable layer penetrates the wholly supersonic region, it is deflected. Thus, our conclusions on the gross stability of the beam rest on our assumption that a vortex-sheet is an adequate representation of its outer boundary.

b) Flow Boundary Conditions

The flow boundary conditions are summarized in Fig. 1. The outflow boundary on the left and the pressure boundary on the top of the grid require some justification and explanation, for they excite a "pressure wave" (see, e.g. Fig. 5) which in late time (e.g. Fig. 4f) interacts with the jet. The outflow condition is used at the left-hand boundary because in some cases cocoon gas must flow out there. The pressure condition is used to keep the shocked IGM gas from overexpanding below the ambient pressure by virtue of the positive radial velocity given the gas at the bow shock. The outflow condition is formulated so that inflow is not permitted should gas next to the boundary begin to flow away from it. In the early stages of jet formation (e.g. Fig. 4a), a rarefaction wave is set up between the bowshock and the left-hand boundary because positive velocities are not allowed on the boundary. As the shock moves on, the rarefaction wave establishes a zone of slightly lower than ambient pressure gas (Fig. 4b), that eventually touches the upper boundary. The upper boundary is maintained at the ambient pressure, which is communicated to the interior via the pressure wave seen especially in Figs. 4d–f, 5, 7, and 8. We believe the pressure wave has little effect on the structure and stability properties of the Mach 1.5 and Mach 3 jets, for the wave is rather weak. In the $\varrho_b=1$, $M_b=6$ jet, the cocoon has already begun to "roll-up" from Kelvin-Helmholtz instabilities before the pressure wave hits the jet. In the $\varrho_b=0.1$, $M_b=6$ jet, the cocoon becomes unstable just as the pressure wave sweeps it (see Fig. 4d–f), however for another reason. As described in Sect. VI, the cocoon is supported by a supersonic backflow from the working surface, which leaves the grid in Fig. 4d. When this happens, the cocoon decelerates to subsonic velocities whereupon it goes KH unstable. In all cases the only effect of the pressure wave is to bring the pressure exerted on the jet back up to the ambient IGM pressure. None of our conclusions regarding structure and stability of the jets seem to require modification.

References

Abbett, M.: 1971, *AIAA J.* **9**, 512

Adamson, T.C., Nicholls, J.A.: 1959, *J. Aerospace Sci.* **26**, 16

Blandford, R.D., Rees, M.J.: 1974, *Monthly Notices Roy. Astron. Soc.* **169**, 395

Blandford, R.D., Rees, M.J.: 1978, *Physica Scripta* **17**, 265

Blandford, R.D., Ostriker, J.P.: 1978, *Astrophys. J. Letters* **221**, L29

Chang, I.-S., Chow, W.L.: 1974, *AIAA J.* **12**, 1079

Courant, R., Friedrichs, K.O.: 1948, Supersonic Flow and Shock Waves, Springer, New York

Ferrari, A., Trussoni, E., Zaninetti, L.: 1978, *Astron. Astrophys.* **64**, 43

Ferrari, A., Trussoni, E., Zaninetti, L.: 1980, *Monthly Notices Roy. Astron. Soc.* **193**, 469

Ferrari, A., Trussoni, E., Zaninetti, L.: 1981, *Monthly Notices Roy. Astron. Soc.* **196**, 1054

Ferrari, A., Massaglia, S., Trussoni, E.: 1982, *Monthly Notices Roy. Astron. Soc.* **198**, 1065

Fox, J.H.: 1974, *AIAA J.* **12**, 105

Gerwin, R.A.: 1968, *Rev. Mod. Phys.* **40**, 652

Hartmann, J., Lazarus, F.: 1941, *Phil. Mag.* **31**, 35

Ladenburg, R., Van Voorhis, C.C., Winckler, J.: 1949, *Phys. Rev.* **76**, 662

Love, E.S., Grigsby, C.E., Lee, L.P., Woodling, M.J., 1959, NASA Technical Report TR-R-6

Mach, E., Salcher, P.: 1889, *Wien. Ber.* **98**, 1303

Miley, G.: 1980, *Ann. Rev. Astron. Astrophys.* **18**, 165

Moe, M.M., Troesch, B.A.: 1960, *ARS J.* **30**, 487

Nieto, J.-L., Lelièvre, G.: 1982 (preprint)

Norman, M.L.: 1980, Ph. D. Dissertation, University of California at Davis; Lawrence Livermore Laboratory Report UCRL-52946

Owen, F.N., Hardee, P.E., Bignell, R.C.: 1980, *Astrophys. J. Letters* **239**, L11

Rayburn, D.R.: 1977, *Monthly Notices Roy. Astron. Soc.* **179**, 603

Scheuer, P.A.G.: 1974, *Monthly Notices Roy. Astron. Soc.* **166**, 513

Strom, R.G., Willis, A.G.: 1981, Second ESO-ESA workshop on the use of the Space Telescope and Coordinated ground-based research: "Optical Jets in Galaxies", p. 83

Tennekes, H., Lumley, J.L.: 1972, in *A First Course in Turbulence*, MIT Press, p. 1

Wilson, J.R.: 1978, in *Source of Gravitational Radiation*, ed. L. Smarr, Cambridge University Press, p. 423

© European Southern Observatory • Provided by the NASA Astrophysics Data System